JOURNAL OF MECHANICAL ENGINEERING AND SCIENCES
ISSN: 2289-4659 e-ISSN: 2231-8380
VOLUME 17, ISSUE 4, 2023, 9715 – 9724
DOI: https://doi.org/10.15282/jmes.17.4.2023.5.0769

UNIVERSITI MALAYSIA PAHANG AL-SULTAN ABDULLAH

RESEARCH ARTICLE

Investigation of the aerodynamic effects of bio-inspired modifications on airfoil at low Reynolds number

H. Demir*, B. Kaya

Department of Mechanical Engineering, Aksaray University, 68100 Aksaray, Turkey
Phone: +903822883685; Fax: +903822883525

ABSTRACT - A numerical study was performed to investigate flow behaviors around bio-inspired modified airfoils compared with NACA 4412 airfoil at Re=5.8x10^4 by solving the two-dimensional, RANS equations with k-ω STT turbulence model. The obtained results reveal a rather abrupt decrease of lift at stall for the NACA 4412 airfoil in contrast to the mild stall depicted by the top-modified airfoil. As compared to the experimental results of the profiled airfoil in the literature, the characteristic behavior of the variation in the lift coefficient shows resemblance. It is seen that from the velocity distribution results, fluid flowed smoothly along the streamlined nose of NACA 4412 airfoil until α=4º and streamlines adhered well for both airfoils at low angles (0º, 2º). Smaller circulation bubbles were noticed to settle in the canyons of the corrugated cross-section of the top-modified airfoil. In the wake region of the modified airfoil, there is no obvious large flow separation or circulation region at low angles of attack. However, the blue regions of the dimensionless velocity over the NACA 4412 airfoil and bottom-modified airfoil were narrower than over the top-modified airfoil. The recirculation zone over the airfoil started to enlarge, and the rolling up of the trailing-edge vortex appeared. After α=12º, the adverse pressure gradient on the suction side of the airfoils became more intense. In the wake zones, it was seen that the circulation regions grew remarkably and became largest as the angle of attack rose to α=16º, which pointed out increased drag forces of airfoils.

ARTICLE HISTORY
Received : 31st May 2023
Revised : 12th Sept. 2023
Accepted : 26th Nov. 2023
Published : 26th Dec. 2023

KEYWORDS
Airfoil
Aerodynamics
Bio-inspired airfoil
CFD
Corrugated
Dragonfly
Low-Reynolds number

1.0 INTRODUCTION

Both designers and engineers commonly seek inspiration to figure out their problems. Nature is the most important source of imagination and inspiration, and this inspiration has helped to solve humanity's numerous matters through biological forms and mechanisms. This tendency has formerly not been apparent in the industrial design area, but there have been substantial initiatives to use nature for inspiration of design latterly. This implementation is attributed to as 'biomimicry'; an innovation inspired by nature [1, 2]. Recently, bio-inspired modification, in engineering design has withdrawn considerable attention, for refinement of flying performance at low Reynolds numbers, particularly in wind turbines, Micro-Air Vehicles (MAV) and Unmanned-Aerial Vehicles (UAV) [3]. Flow separation and stall phenomena represent adverse occurrences within low Reynolds number flow environments, resulting in diminished aerodynamic performance. Consequently, endeavors have been undertaken to mitigate flow separation and stall phenomena through the implementation of flow control methodologies. These methods have been broadly categorized into two distinct branches: active control and passive control techniques. Nowadays, passive control techniques have garnered preference over their active counterparts due to their inherent energy efficiency [4]. A selection of these controllers can be organized such as vortex generators [5–8], employing roughness material [9, 10], using flexibility [11–20], utilizing the dimple [21], riblet [22, 23], considering the bio-inspired tubercles [24–29] and performing bio-inspired applications [30–32].

As previously elucidated, bio-inspiration from nature has led to numerous innovative aerodynamic designs and concepts because nature presents efficient, vigorous, and straightforward remedies for engineering problems. Additionally, nature serves us distinguished samples of flight from varied aspects, such as optimum energy consumption at intense agility motions, stability, and low noise. One of the most impressive flying kinds is insect flight. Dragonflies have diverse flight characteristics and excellent maneuvering capabilities. They can move directly up or down, hover and fly backward. The wings of dragonflies consist of a corrugated cross-section with camber. The wing cross-sections display distinct and precisely defined corrugated configurations as illustrated in Figure 1. This corrugated pattern is crucial in aerodynamic performance [33, 34]. Several studies were concerned with dragonflies experimentally and numerically. Murphy and Hu [35] investigated the aerodynamic qualifications of bioinspired corrugated airfoil compared with a smooth-surfaced airfoil and a flat plate to detect the possible implementations of such bio-inspired corrugated airfoils for MAV experimentally. It was noticed that the corrugated airfoil has better performance over the flat plate and smooth-surfaced airfoil in terms of higher lift and inhibiting large-scale flow separation. Additionally, it was found that the corrugated airfoil was nearly irresponsive to the Re numbers in terms of aerodynamic performance. The same observations were also found by Tamai et al. [36].

***CORRESPONDING AUTHOR | H. Demir** | ✉ hmdemir@aksaray.edu.tr

Hu and Tamai [37] investigated and compared flow behavior around flat plate, normal GA(W)-1 airfoil and dragonfly airfoil experimentally. As a result of the studies, GA(W)-1 airfoil performed better up to 10 degrees, while the dragonfly wing geometry was more successful after 10 degrees. Additionally, A. Shahzad et al. [38] performed numerical analysis using the geometry of dragonfly wings, which they modified in different ways. As a result of the CFD study, the smooth transition of the upper part of the dragonfly wing geometry and the preservation of the lower part of the dragonfly wing geometry gave better results in all other dragonfly wing geometry. Dwivedi et al. [39] created two different dragonfly wing geometries and combined the points of one of these geometries to form a wing. They performed an experimental and numerical examination of these three different wing types. The result stated that hybrid airfoil was proper just for up to 4º. The modified simple corrugated airfoil displayed important aerodynamic performance compared to the other tested airfoils at high angles of attack.

Sooraj and Agrawal [40] performed numerical analysis by modeling dragonfly wings. One of the remarkable points is that he made this analysis based on time. This study showed us why the dragonfly wing should operate at lower Reynolds numbers than normal wings. On the other hand, Mahmoud E Abd El-Latief et al. [41] created a dragonfly wing geometry and a flat plate geometry, and in addition, a new wing was formed by connecting the points in the dragonfly wing geometry. All wings were analyzed numerically. The most successful wing in terms of aerodynamics was the original dragonfly wing. Additionally, Kharati-koopaee and Fallahzadeh-abarghooee [42] examined the influence of corrugated skins on the aerodynamic performance of various cambered airfoils with considering diverse factors such as Reynolds numbers, maximum cambers and their locations, corrugation numbers and amplitudes. The analysis focuses on evaluating the impact of these factors on slope of mean lift curve and drag coefficient, in comparison to relevant smooth portions. While morphing skins hold potential for enhancing aircraft abilities, the computational results reveal that the introduction of corrugated skins mostly leads to a degradation in the aerodynamic performance of the airfoil sections. At low corrugation amplitudes, the impact of increasing Reynolds number and maximum camber on the relative zero-incidence drag coefficient is found to be of minimal matter.

In their numerical study, Harbig et al. [43] examined the influence of the aspect ratio of wing and Reynolds number on flow behaviors on insect-like wings. The simulations demonstrated that both augmenting the Reynolds number for an aspect ratio of 2.91 and augmenting the aspect ratio at constant Reynolds numbers ranging from 120 to 1500 yielded similar impacts on flow patterns, resulting in an augmentation of the lift coefficient. Flint and Jermy [44] conducted a two-dimensional numerical study on the aerodynamic efficiency of a pitching bioinspired corrugated airfoil and analyzed the attributes of the viscous flow surrounding it. The wing shape utilized in their study was observed to cause the viscous features developed on the upper surface of the wing to display a significant sensitivity to the oscillating conditions, ultimately impacting the wing's overall performance. It was revealed that the corrugated airfoil demonstrated the capability to generate thrust force under specific conditions characterized at k=4.96 and A=20º. Vargas et al. [45] conducted a computational study focusing on analyzing the aerodynamic performance of a dragonfly wing section during the gliding flight. They conducted simulations not only for the pleated wing but also for its smoothed counterpart and a flat plate. The purpose was to gain insights into the aerodynamic characteristics of the pleated wing by comparing it with other wing designs. It was revealed that the pleated airfoil exhibited similar, and in certain cases, even higher lift compared to the profiled airfoil. Additionally, it was found that the drag characteristics of the pleated airfoil were comparable to those of the profiled airfoil. The concurrent enhancement in lift and the modest drag exhibited by the pleated airfoil led to an aerodynamic performance that was at least equivalent to, and occasionally even superior to, that of the profiled airfoil. These findings highlight the favorable aerodynamic attributes of the pleated wing design.

To the best of our knowledge, no study has investigated the aerodynamic impact of bio-inspired modifications on both the suction and pressure surfaces of the NACA 4412 airfoil, specifically using the corrugated dragonfly wing geometry. Therefore, this study aims to conduct a numerical investigation into the flow behaviors of a NACA 4412 airfoil, which has been subjected to bio-inspired modifications. Additionally, the primary objective is to analyze the aerodynamic characteristics of the modified airfoils at a constant Reynolds number of 5.8×10^4. The study also includes a comparative analysis of various angles of attack with a previously conducted experimental study in the literature.

2.0 NUMERICAL METHODOLOGY

This study represents the flow characteristics of NACA 4412 airfoil having bio-inspired modifications which are placed on its both pressure and suction sides. The geometric bio-inspired modifications on NACA 4412 airfoil were established by considering a representative cross-section of the dragonfly wing previously studied by Murphy and Hu [35], Hu and Tamai [37] as seen in Figure 2(a). The modifications made to the airfoil were designed in a manner that preserves the outline of the original NACA 4412 airfoil. The geometry of the corrugated dragonfly airfoil coincides with the fore-wing of a dragonfly Aeshna cyanea gained at the midsection of the wing, which was digitally extracted from the profiles provided in Kesel [46]. In this study, 2-D, steady-state numerical simulations were performed by solving Reynolds-Averaged Navier-Stokes (RANS) equations with k-ω STT turbulence model by utilizing the ANSYS Fluent. This turbulence model is recognized as an efficacious transitional approach, particularly proficient at capturing the intricacies of fluid dynamics characterized by low Reynolds number flows [47, 48]. The geometries of the airfoils were designed using SOLIDWORKS software. In the design, which is shown in Figure 2, the chord length (C) is 0.101 m based on the corrugated dragonfly airfoil.

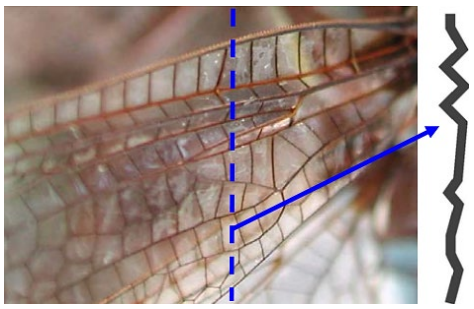

Figure 1. Corrugated cross-section of a dragonfly wing [36]

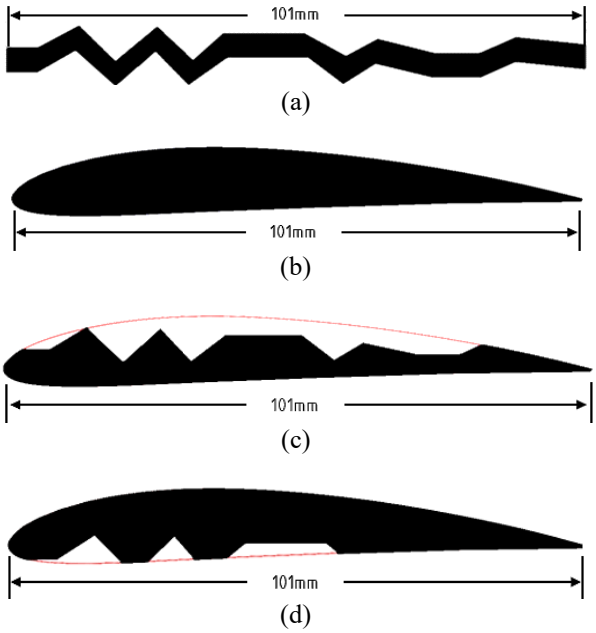

Figure 2. Schematic view of the airfoils: (a) Corrugated dragonfly airfoil [35, 36], (b) NACA 4412 airfoil, (c) Top-modified airfoil and (d) Bottom-modified airfoil

2.1 Computational Grid and Boundary Conditions

The flow domain, computational mesh and boundary conditions were selected to be identical for unique benchmark of both the flow and aerodynamic characteristics of the NACA 4412 airfoil, as well as top and bottom-modified airfoils inspired by dragonfly, as depicted in Figure 3. The computational mesh was divided into a C-type structural mesh. In order to capture the sophisticated flow characteristics of airfoils, dimensions of the domain were restrained to 17C in the streamwise direction and 10C in the cross direction. Additionally, the leading edge of the airfoil was settled at a distance of 5C, while the domain was enlarged up to 12C from the trailing edge. To resolve the boundary layer favorably and hereby to capture the complicated flow features, fine mesh was generated in the vicinity of the airfoil and coarse mesh was constituted distant from the body, where the flow impacts are nearly neglectable. For pressure-velocity coupling, the COUPLED algorithm was utilized. Additionally, the least squares cell-based method was selected for gradient and for all other parameters second-order upwind method was utilized. Convergence of the computations was obtained when residuals were lower than 10^{-6}.

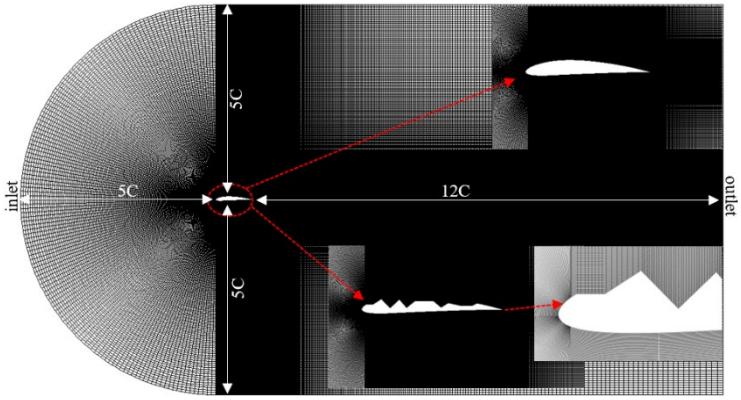

Figure 3. The computational grid, domain, and boundary conditions

2.2 Flow Control Equation and Turbulence Model

The governing equations for incompressible, Newtonian fluid flow based on the Reynolds-Averaged Navier-Stokes (RANS) approach used in this study are summarized as following:

The continuity equation is:

$$\frac{\partial u_i}{\partial x_i} = 0 \tag{1}$$

The momentum equation is:

$$\frac{\partial u_i}{\partial t} + \frac{\partial}{\partial x_j}(u_i u_j) = -\frac{1}{\rho}\frac{\partial p}{\partial x_i}\left[\nu\left(\frac{\partial u_i}{\partial x_j} + \frac{\partial u_i}{x_i}\right)\right] + \tau_{ij} \tag{2}$$

where, t and x_i denote the time and space Cartesian coordinates, u_i u_i and u_j denote flow velocity components. p, ρ and ν denote pressure, density, and kinematic viscosity.

The Shear Stress Transport (SST) k-ω turbulence model is a widely used two-equation turbulence model in CFD simulations. It is an extension of the Wilcox k-ω turbulence model, which combines aspects of the k-ε and k-ω models to provide improved accuracy and robustness for a variety of flow situations. This turbulence model is suitable to simulate the boundary layer and complex turbulent flow field that includes unsteadiness and separation. The SST k-ω turbulence model is defined as following Eqs. (3) and (4).

$$\frac{\partial(\rho k)}{\partial t} + \frac{\partial}{\partial x_j}(\rho u_j k) = \frac{\partial}{\partial x_j}\left[(\mu + \sigma_k \mu_t)\frac{\partial k}{\partial x_j}\right] + P_k - \beta\rho\omega k \tag{3}$$

$$\frac{\partial(\rho\omega)}{\partial t} + \frac{\partial}{\partial x_j}(\rho u_j \omega) = \frac{\partial}{\partial x_j}\left[\mu + \sigma_\omega \mu_t \frac{\partial \omega}{\partial x_j}\right] + 2(1-F_1)\rho\sigma_{\omega 2}\frac{1}{\omega}\frac{\partial k}{\partial x_j}\frac{\partial \omega}{\partial x_j} + \alpha\frac{\omega}{k}P_k - \beta\rho\omega^2 \tag{4}$$

In Eq. (3), the term denoting the production of turbulence (P_k), herein referred to as (τ_{ij}), may be expounded upon by invoking the formulations elucidated in Eqs. (5) and (6) as follows.

$$P_k = \tau_{ij}\frac{\partial u_i}{\partial x_j} \tag{5}$$

$$\tau_{ij} = \mu_i\left(\frac{\partial u_i}{\partial x_j} + \frac{\partial u_i}{\partial x_j} - \frac{2}{3}\delta_{ij}\frac{\partial u_i}{\partial x_j}\right) - \frac{2}{3}\rho k\delta_{ij} \tag{6}$$

The blending functions, F_1 and F_2 are given as following Eqs. (7) and (8).

$$F_1 = \tanh\left\{\left\{\min\left[\max\left(\frac{\sqrt{k}}{0.09\omega y}, \frac{500\nu}{y^2\omega}\right), \frac{4\rho k}{\sigma_{\omega,2}D_\omega^+ y^2}\right]\right\}^4\right\} \tag{7}$$

$$F_2 = \tanh\left[\left[\max\left(2\frac{\sqrt{k}}{0.09\omega y}, \frac{500\nu}{y^2\omega}\right)\right]^2\right] \tag{8}$$

where, is y the distance to the next surface and D_ω^+ is the positive portion of the cross-diffusion term. Turbulent viscosity is defined as Eq. (9) for SST k-ω model.

$$\nu_t = \frac{0.31k}{\max(0.31\omega, \Omega F_2)}; \quad \Omega = \left|\frac{\partial v}{\partial x} - \frac{\partial u}{\partial y}\right| \tag{9}$$

3.0 RESULTS AND DISCUSSION

3.1 Numerical Aerodynamic Coefficients

The stall characteristics were studied from the lift coefficient (C_L) and drag coefficient (C_D) of the NACA 4412 airfoil and modified airfoils inspired by dragonfly for different angles of attack starting from α=0º to α=24º. The lift coefficients for NACA 4412 airfoil and modified airfoils at chord Reynolds number of $5.8\text{x}10^4$ are depicted in Figure 4. The stall angles for both NACA 4412 airfoil and modified airfoils were found to be α=12º. There is also a remarkable reduction

in C_{Lmax} for the top-modified airfoil in comparison to the NACA 4412 airfoil and bottom-modified airfoil. The NACA 4412 airfoil and bottom-modified airfoil both stalls abruptly in a single stage, whereas the top-modified airfoil stalls progressively in several stages. As compared to the profiled airfoil used by Murphy and Hu [35] in their experimental study, the characteristic behavior of the variation in the lift coefficient shows similarity.

Additionally, it is realized that at the top-modified airfoil has a remarkably greater drag (C_D) than the NACA 4412 airfoil and the bottom-modified airfoil up to α=20º. As the angle of attack further increases beyond α=20º, the difference in drag values between the airfoils starts to decline and remains almost the same for both airfoils. The NACA 4412 airfoil experiences a higher C_L in the pre-stall region, but this drops off suddenly after reaching the stall angle. By virtue of the existence of corrugated surfaces, the stall happens progressively for the top-modified airfoil. The obtained results reveal a rather abrupt decrease of lift at the stall for the NACA 4412 airfoil in contrast to the mild stall depicted by the top-modified airfoil.

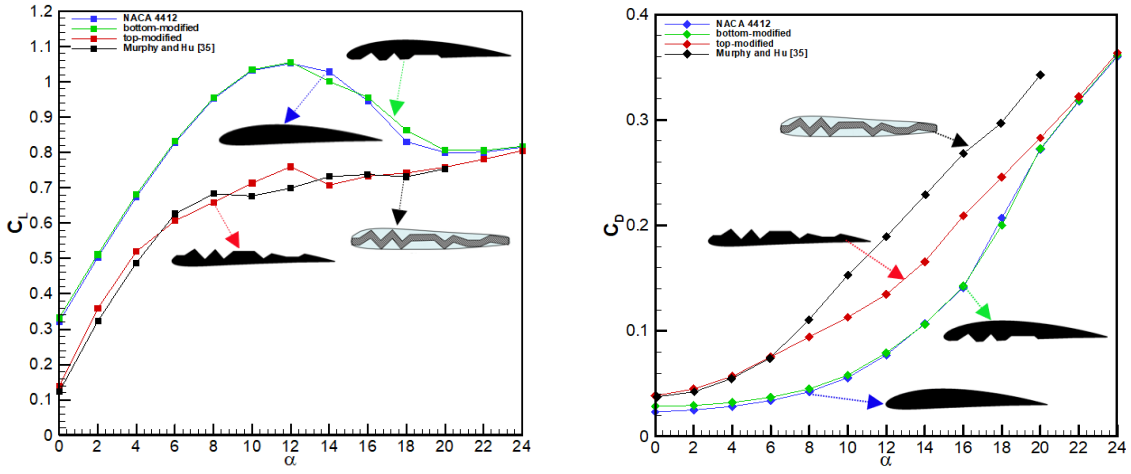

(a) (b)

Figure 4. Aerodynamic force coefficients of airfoils: (a) Lift coefficient and (b) Drag coefficient

3.2 Velocity Distributions

The comparison of dimensionless velocity distributions with streamlines of NACA 4412 airfoil and modified airfoils at a fixed Re value of $5.8x10^4$ for varied angles of attack is shown in Figure 5. Fluid flowed smoothly along the streamlined nose of the NACA 4412 airfoil until α=4º and it can be stated that streamlines adhered well for all airfoils at low angles (0º, 2º). Separation in the trailing-edge started to form on the upper side of the NACA 4412 airfoil at α=4º and enlarged with increasing angle of attack. Because of the separation, the dimensionless velocity was less around the aft of all airfoils and the blue region (lower velocity) increased with increasing the angle of attack. The laminar shear layer happened in the top-modified airfoil because arriving fluid flow separated from the sharp leading edge of the top-modified airfoil. The occurrence of circulation bubble close to the leading-edge of the bioinspired the top-modified airfoil was seen obviously as given in Figure 5. The presence of reduced scale vortical structures was observed to localize within the concave regions of the corrugated cross-sectional profile. Speedy fluid streams outwards the corrugation canyons were noticed to stream sightly throughout a virtual envelope profile. In the wake region of the top-modified airfoil, there was no obvious large flow separation or circulation region at low angles of attack. The streamlines pattern demonstrated that vortices were trapped in corrugated valley and also flow passing on the modified airfoil was similar to the flow on the smooth airfoil. The flow separation happened from downstream of the tip of one corrugation and reattached to the upstream tip of next corresponding corrugation. Additionally, stream-wise velocity contours showed that reverse flow and blue region were grown gradually along the suction side of all airfoils with the rising angle of attack. However, the blue region of the dimensionless velocity over the NACA4412 airfoil and bottom-modified airfoil was narrower than over the top-modified airfoil. As illustrated in Figure 5(d) (α=12º), a large recirculation zone happened over the airfoil, and the rolling up of the trailing-edge vortex appeared. After α=12º, significant flow separation was observed across a substantial portion of the upper surface of the airfoils, resulting in aerodynamic stall conditions. This phenomenon led to the development of an expanded circulation region in the wake region of the airfoils. With an increase in the angle of attack, the adverse pressure gradient on the suction side of the airfoils became more intense. In the wake zones, it was seen that the circulation regions grew remarkably as the angle of attack rose to α=16, which pointed out increased drag forces of airfoils. On account of the strong adverse pressure gradient at α=16, high-speed flow streams around the top-modified airfoil could no longer trace the corrugated cross-sectional envelope profile.

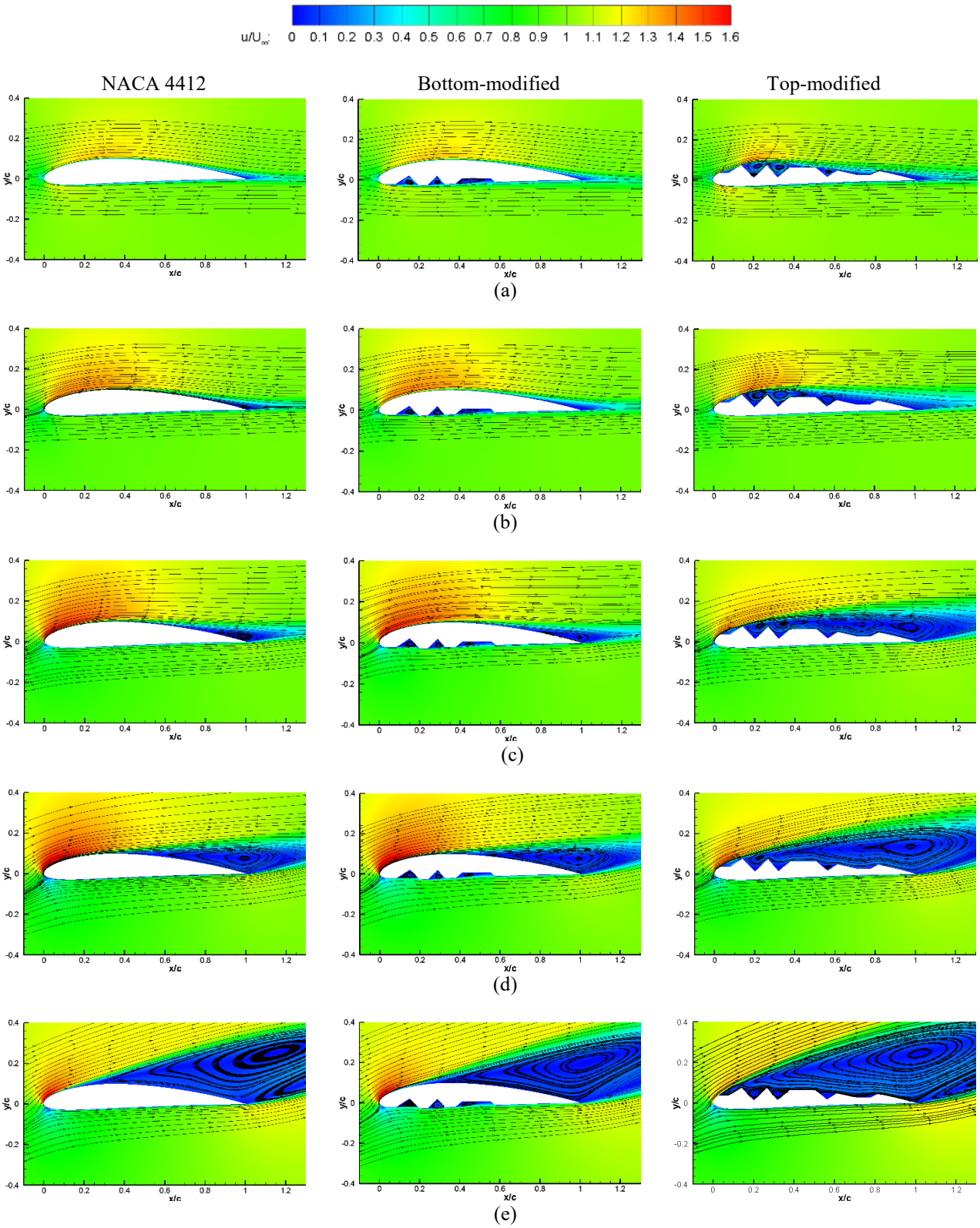

Figure 5. Dimensionless velocity distributions around the airfoils: (a) α=0º, (b) α=4º, (c) α=8º, (d) α=12º, and (e) α=16º

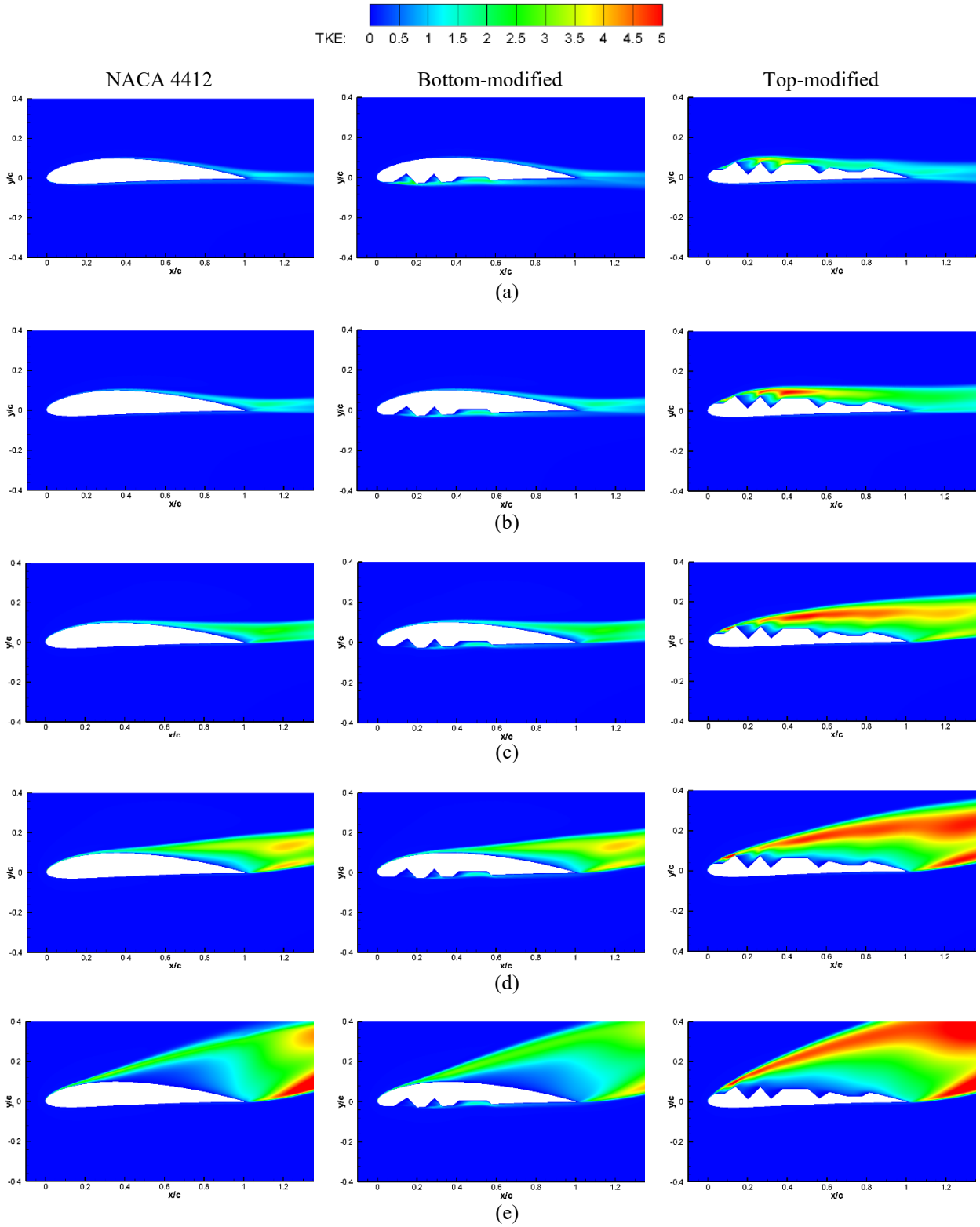

Figure 6. Turbulent kinetic energy distributions around the airfoils: (a) α=0º, (b) α=4º, (c) α=8º, (d) α=12º, and (e) α=16º

Figure 6 displays the contours of turbulent kinetic energy on airfoils, providing insight into the distribution characteristics. The color gradient represented in the figures indicates the varying values of turbulent kinetic energy across the airfoil surfaces. The color spectrum employed ranges from blue, denoting the minimum values, to red, symbolizing the maximum values. At zero angle, the turbulent kinetic energy exhibits a concentrated presence in a localized region near the trailing edge. However, with an increase in the angle of attack, the magnitude of turbulent kinetic energy escalates adjacent to the trailing edge, subsequently propagating across the upper surface of the airfoil. Consequently, it can be inferred that the turbulent kinetic energy distribution illustrates a comparable behavior up to the point of reaching the stall angle, which is estimated to be approximately 12 degrees for both the NACA 4412 airfoil and the bottom-modified airfoil. At an angle of attack of 16 degrees, a distinct wake region emerges above the upper surface of the airfoil, exhibiting a significantly reduced level of turbulent kinetic energy. Conversely, beyond this wake region, an elevated magnitude of

turbulent kinetic energy becomes discernible. This distinctive behavior can be attributed to the turbulence generated as a consequence of flow separation phenomena occurring in the flow field. In contrast to the previous case, there is a notable escalation in the intensity of the red zone observed on the upper surface of the airfoil, accompanied by the formation of a substantial wake zone. This observation is consistent with the anticipated behavior, affirming the increase in turbulent kinetic energy within this case.

4.0 CONCLUSIONS

In this study, the flow behaviors of NACA 4412 airfoil having bio-inspired modifications were numerically investigated at a constant Reynolds number of 5.8×10^4. In summary, the findings of this study shed light on the aerodynamic behavior of the NACA 4412 airfoil and bio-inspired modified airfoils. The modified airfoils, inspired by the corrugated structure of a dragonfly wing, exhibited unique stall characteristics and flow patterns compared to the conventional NACA 4412 airfoil. The stall behavior of the airfoils differed significantly. The top-modified airfoil experienced a progressive stall in multiple stages, whereas the NACA 4412 airfoil and bottom-modified airfoil had a sudden stall in a single stage. This indicates that the presence of corrugations on the top surface of the airfoil influenced the stall progression. Furthermore, the drag values of the top-modified airfoil were higher than those of the other airfoils, up to $\alpha=20^o$. This suggests that the corrugated structure on the top surface increased the drag forces experienced by the airfoil.

The flow patterns and separation phenomena were examined to understand the aerodynamic performance. At low angles of attack, the flow adhered well to the airfoil surfaces, but as the angle of attack increased, separation and circulation regions appeared. The corrugated structure of the top-modified airfoil induced a laminar shear layer and influenced the separation and reattachment processes. The distribution of turbulent kinetic energy provided further insights into the flow characteristics. The turbulent kinetic energy intensified near the trailing edge and propagated across the upper surface of the airfoils as the angle of attack increased. A distinct wake region with reduced turbulent kinetic energy was observed above the airfoil surface at an angle of attack of 16 degrees, indicating the presence of turbulence generated by flow separation. Overall, this study highlights the significance of geometric modifications in airfoil design and their impact on aerodynamic performance. The bio-inspired modifications demonstrated unique stall behavior and altered flow patterns, emphasizing the potential for improving airfoil performance through nature-inspired designs. These findings could contribute to the field of aerodynamics and provide valuable insights for future research and the development of more efficient and high-performance airfoil designs.

5.0 NOMENCLATURE

CFD	Computational Fluid Dynamics	P_k	Production of turbulence
MAV	Micro Air Vehicle	Re	Reynolds number
UAV	Unmanned-Aerial Vehicles	t	Time
RANS	Reynolds-Averaged Navier-Stokes	U_∞	Free-stream velocity
SST	Shear Stress Transport	y	Distance to the next surface
TKE	Turbulent Kinetic Energy	α	Angle of attack
C	Airfoil chord length	β	Turbulence modeling constant
C_L	Lift coefficient	ρ	Density
C_D	Drag coefficient	μ	Viscosity
D_ω^+	Positive portion of the cross-diffusion term	μ_t	Eddy viscosity
F_1	Blending function	ν	Kinematic viscosity
F_2	Blending function	ω	Specific turbulent dissipation rate
k	Specific turbulent kinetic energy		
p	Pressure		

6.0 REFERENCES

[1] S. Kennedy, "Biomimicry/biomimetics: General principles and practical examples," *The Science Creative Quarterly* [Online], Accessed: December 2023. Available: https://www.scq.ubc.ca/biomimicrybimimetics-general-principles-and-practical-examples/

[2] N. L. Volstad and C. Boks, "On the use of biomimicry as a useful tool for the industrial designer," *Sustainable Development*, vol. 20, no. 3, pp. 189–199, 2012.

[3] P. C. Khandelwal and T. L. Hedrick, "Combined effects of body posture and three-dimensional wing shape enable efficient gliding in flying lizards," *Scientific Reports*, vol. 12, p. 1793, 2022.

[4] M. Serdar Genç, K. Koca, H. Demir, and H. Hakan Açıkel, "Traditional and new types of passive flow control techniques to pave the way for high maneuverability and low structural weight for UAVs and MAVs," *Autonomous Vehicles*, pp. 131-160, 2020.

[5] M. Özden, M. S. Genç, and K. Koca, "Investigation of the effect of hidden vortex generator-flap integrated mechanism revealed in low velocities on wind turbine blade flow," *Energy Conversion and Management*, vol. 287, p. 117107, 2023.

[6] X. K. Li, W. Liu, T. J. Zhang, P. M. Wang, and X. D. Wang, "Experimental and numerical analysis of the effect of vortex generator installation angle on flow separation control," *Energies*, vol. 12, no. 23, p. 4583, 2019.

[7] R. Jiang *et al*., "Effect of vortex generator orientation on wind turbines considering the three-dimensional rotational effect," *Ocean Engineering*, vol. 267, p. 113307, 2023.

[8] Y. Liu, H. Zhe, Y. Xue, J. Tan, P. Yuan, and Q. Zhang, "Effects of vortex generator on the hydrodynamic characteristics of hydrofoil and horizontal axis tidal turbine," *Physics of Fluids*, vol. 35, p. 035104, 2023.

[9] F. R. Marzabadi and M. R. Soltani, "Effect of leading-edge roughness on boundary layer transition of an oscillating airfoil," *Scientia Iranica*, vol. 20, no. 3, pp. 508–515, 2013.

[10] M. Serdar Genç, K. Koca, and H. H. Açıkel, "Investigation of pre-stall flow control on wind turbine blade airfoil using roughness element," *Energy*, vol. 176, pp. 320–334, 2019.

[11] M. Tamai, J. T. Murphy, and H. Hu, "An experimental study of flexible membrane airfoils at low Reynolds numbers," *46th AIAA Aerospace Sciences Meeting and Exhibit*, Reno, United States, Jan. 7-10, 2008.

[12] P. Rojratsirikul, M. S. Genc, Z. Wang, and I. Gursul, "Flow-induced vibrations of low aspect ratio rectangular membrane wings," *Journal of Fluids and Structures*, vol. 27, no. 8, pp. 1296–1309, 2011.

[13] S. Arbós-Torrent, B. Ganapathisubramani, and R. Palacios, "Leading- and trailing-edge effects on the aeromechanics of membrane aerofoils," *Journal of Fluids and Structures*, vol. 38, pp. 107–126, 2013.

[14] M. S. Genç, H. H. Açikel, H. Demir, M. Özden, M. Çağdaş, and I. Isabekov, "Effect of tip vortices on membrane vibration of flexible wings with different aspect ratios," in *EPJ Web of Conferences*, vol. 114, p. 02028, 2016.

[15] M. S. Genç, M. Özden, H. H. Açikel, H. Demir, and I. Isabekov, "Unsteady flow over flexible wings at different low Reynolds numbers," in *EPJ Web of Conferences*, vol. 114, p. 02030, 2016.

[16] H. Demir and M. S. Genç, "An experimental investigation of laminar separation bubble formation on flexible membrane wing," *European Journal of Mechanics - B/Fluids*, vol. 65, pp. 326–338, 2017.

[17] A. Shahzad, F. B. Tian, J. Young, and J. C. S. Lai, "Effects of flexibility on the hovering performance of flapping wings with different shapes and aspect ratios," *Journal of Fluids and Structures*, vol. 81, pp. 69–96, 2018.

[18] H. H. Açıkel and M. Serdar Genç, "Control of laminar separation bubble over wind turbine airfoil using partial flexibility on suction surface," *Energy*, vol. 165, pp. 176–190, 2018.

[19] M. S. Genç, H. Demir, M. Özden, and T. M. Bodur, "Experimental analysis of fluid-structure interaction in flexible wings at low Reynolds number flows," *Aircraft Engineering and Aerospace Technology*, vol. 93, no. 6, pp. 1060–1075, 2021.

[20] K. Koca, M. S. Genç, E. Bayır, and F. K. Soğuksu, "Experimental study of the wind turbine airfoil with the local flexibility at different locations for more energy output," *Energy*, vol. 239, p. 121887, 2022.

[21] S. Roy, A. Biswas, B. Das, and B. V Reddy, "Flow control of a wind-turbine airfoil with a leading-edge spherical dimple," *International Journal of Green Energy*, vol. 20, no. 12, pp. 1307–1325, 2023.

[22] J. M. Caram and A. Ahmed, "Effect of riblets on turbulence in the wake of an airfoil," *AIAA Journal*, vol. 29, no. 11, pp. 1769–1770, 1991.

[23] Y. Zhang, H. Chen, S. Fu, and W. Dong, "Numerical study of an airfoil with riblets installed based on large eddy simulation," *Aerospace Science and Technology*, vol. 78, pp. 661–670, 2018.

[24] Z. Wei, T. H. New, and Y. D. Cui, "An experimental study on flow separation control of hydrofoils with leading-edge tubercles at low Reynolds number," *Ocean Engineering*, vol. 108, pp. 336–349, 2015.

[25] C. J. Bai, Y. Y. Lin, S. Y. Lin, and W. C. Wang, "Computational fluid dynamics analysis of the vertical axis wind turbine blade with tubercle leading edge," *Journal of Renewable and Sustainable Energy*, vol. 7, no. 3, 2015.

[26] I. K. A. P. Utama *et al*., "Numerical simulation of foil with leading-edge tubercle for vertical-axis tidal-current turbine," *Journal of Mechanical Engineering and Sciences*, vol. 14, no. 3, pp. 6982–6992, 2020.

[27] Y. Zhang *et al.*, "Investigation of aerodynamic forces and flow field of an H-type vertical axis wind turbine based on bionic airfoil," *Energy*, vol. 242, p. 122999, 2022.

[28] M. Fan, Z. Sun, X. Dong, and Z. Li, "Numerical and experimental investigation of bionic airfoils with leading-edge tubercles at a low-Re in considering stall delay," *Renewable Energy*, vol. 200, pp. 154–168, 2022.

[29] S. Roy, B. Das, and A. Biswas, "A comprehensive review of the application of bio-inspired tubercles on the horizontal axis wind turbine blade," *International Journal of Environmental Science and Technology*, vol. 20, no. 4, pp. 4695–4722, 2023.

[30] K. L. Hansen, R. M. Kelso, and B. B. Dally, "Performance variations of leading-edge tubercles for distinct airfoil profiles," *AIAA Journal*, vol. 49, no. 1, pp. 185–194, 2011.

[31] J. Wang, T. Nakata, and H. Liu, "Development of mixed flow fans with bio-inspired grooves," *Biomimetics*, vol. 4, no. 72, pp. 1-19, 2019.

[32] S. Huang, H. Qiu, and Y. Wang, "Aerodynamic performance of horizontal axis wind turbine with application of dolphin head-shape and lever movement of skeleton bionic airfoils," *Energy Conversion and Management*, vol. 267, p. 115803, 2022.

[33] Q. Li, M. Zheng, T. Pan, and G. Su, "Experimental and numerical investigation on dragonfly wing and body motion during voluntary take-off," *Scientific Reports*, vol. 8, no. 1, pp. 1–16, 2018.

[34] G. R. Abdizadeh, M. Farokhinejad, and S. Ghasemloo, "Numerical investigation on the aerodynamic efficiency of bio-inspired corrugated and cambered airfoils in ground effect," *Scientific Reports,* vol. 12, no. 1, pp. 1–19, 2022.

[35] J. T. Murphy and H. Hu, "An experimental study of a bio-inspired corrugated airfoil for micro air vehicle applications," *Experiments in fluids*, vol. 49, no. 2, pp. 531–546, 2010.

[36] M. Tamai, W. Zhijian, G. Rajagopalan, H. Hui, and H. Guowei, "Aerodynamic performance of a corrugated dragonfly airfoil compared with smooth airfoils at low reynolds numbers," in *Collection of Technical Papers-45th AIAA Aerospace Sciences Meeting*, pp. 5800–5811, 2007.

[37] H. Hui and M. Tamai, "Bioinspired corrugated airfoil at low Reynolds numbers," *Journal of Aircraft*, vol. 45, no. 6, pp. 2068–2077, 2008.

[38] A. Shahzad, H. R. Hamdani, and A. Aizaz, "Investigation of corrugated wing in unsteady motion," *Journal of Applied Fluid Mechanics*, vol. 10, no. 3, pp. 833–845, 2017.

[39] Y. D. Dwivedi, S. Y. B. Sudhir, B. Sunil, C. H. V. K. N. S. N. Moorthy, and K. V. Allamraju, "Numerical study of bio-inspired corrugated airfoil geometry in a forward flight at a low Reynolds number," *WSEAS Transactions on Fluid Mechanics*, vol. 17, pp. 119–127, 2022.

[40] P. Sooraj and A. Agrawal, "Passive flow control mechanism in a bio-inspired corrugated hydrofoil," *SN Applied Sciences*, vol. 1, no. 11, pp. 1–17, 2019.

[41] M. E. Abd El-Latief, K. Elsayed, and M. Madbouli Abdelrahman, "Aerodynamic study of the corrugated airfoil at ultra-low Reynolds number," *Advances in Mechanical Engineering*, vol. 11, no. 10. pp. 1–18, 2019.

[42] M. Kharati-koopaee and M. Fallahzadeh-abarghooee, "Effect of corrugated skins on the aerodynamic performance of the cambered airfoils," *Engineering Computations*, vol. 35, no. 3, pp. 1567–1582, 2018.

[43] R. R. Harbig, J. Sheridan, and M. C. Thompson, "Reynolds number and aspect ratio effects on the leading-edge vortex for rotating insect wing planforms," *Journal of Fluid Mechanics*, vol. 717, pp. 166–192, 2013.

[44] T. J. Flint, M. C. Jermy, T. H. New, and W. H. Ho, "Computational study of a pitching bio-inspired corrugated airfoil," *International Journal of Heat and Fluid Flow*, vol. 65, pp. 328–341, 2017.

[45] A. Vargas, R. Mittal, and H. Dong, "A computational study of the aerodynamic performance of a dragonfly wing section in gliding flight," *Bioinspiration & Biomimetics*, vol. 3, no. 2, p. 26004, 2008.

[46] A. B. Kesel, "Aerodynamic characteristics of dragonfly wing sections compared with technical aerofoils," *Journal of Experimental Biology*, vol. 203, no. 20, pp. 3125–3135, 2000.

[47] H. Demir and B. Kaya, "A study on aerodynamic performance of airfoil in ground effect," in *8th International Asian Congress on Contemporary Sciences*, Aksaray, Turkiye, May 5-7, 2023.

[48] I. Karasu, M. Özden, and M. S. Genç, "Performance assessment of transition models for three-dimensional flow over NACA4412 wings at low Reynolds numbers," *Journal of Fluids Engineering*, vol. 140, no. 12, p. 121102, 2018.